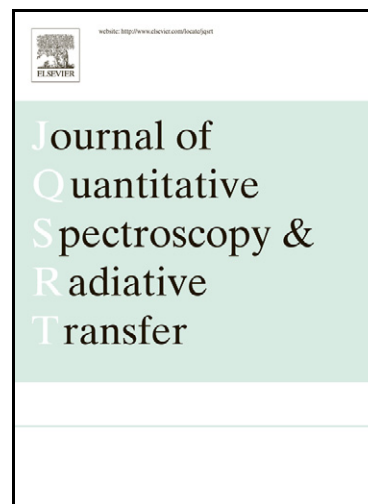


Author's Accepted Manuscript

Modifications Of Discrete Ordinate Method For Computations With High Scattering Anisotropy: Comparative Analysis

Sergey V. Korkin, Alexei I. Lyapustin, Vladimir V. Rozanov



www.elsevier.com/locate/jqsrt

PII: S0022-4073(12)00356-1
DOI: <http://dx.doi.org/10.1016/j.jqsrt.2012.07.022>
Reference: JQSRT4099

To appear in: *Journal of Quantitative Spectroscopy & Radiative Transfer*

Received date: 14 May 2012
Revised date: 18 July 2012
Accepted date: 20 July 2012

Cite this article as: Sergey V. Korkin, Alexei I. Lyapustin and Vladimir V. Rozanov, Modifications Of Discrete Ordinate Method For Computations With High Scattering Anisotropy: Comparative Analysis, *Journal of Quantitative Spectroscopy & Radiative Transfer*, <http://dx.doi.org/10.1016/j.jqsrt.2012.07.022>

This is a PDF file of an unedited manuscript that has been accepted for publication. As a service to our customers we are providing this early version of the manuscript. The manuscript will undergo copyediting, typesetting, and review of the resulting galley proof before it is published in its final citable form. Please note that during the production process errors may be discovered which could affect the content, and all legal disclaimers that apply to the journal pertain.

MODIFICATIONS OF DISCRETE ORDINATE METHOD FOR COMPUTATIONS WITH HIGH SCATTERING ANISOTROPY: COMPARATIVE ANALYSIS

Sergey V. Korkin^{a,b}, Alexei I. Lyapustin^b, Vladimir V. Rozanov^c

^aUniversities Space Research Association GESTAR, Columbia, MD, USA;

^bNASA Goddard Space Flight Center, code 613, Greenbelt, MD, USA;

^cInstitute of Remote Sensing, University of Bremen, Bremen, Germany.

Abstract

A numerical accuracy analysis of the radiative transfer equation (RTE) solution based on separation of the diffuse light field into anisotropic and smooth parts is presented. The analysis uses three different algorithms based on the discrete ordinate method (DOM). Two methods, DOMAS and DOM2+, that do not use the truncation of the phase function, are compared against the TMS-method. DOMAS and DOM2+ use the Small-Angle Modification of RTE and the single scattering term, respectively, as an anisotropic part. The TMS method uses Delta-M method for truncation of the phase function along with the single scattering correction. For reference, a standard discrete ordinate method, DOM, is also included in analysis. The obtained results for cases with high scattering anisotropy show that at low number of streams (16, 32) only DOMAS provides an accurate solution in the aureole area. Outside of the aureole, the convergence and accuracy of DOMAS, and TMS is found to be approximately similar: DOMAS was found more accurate in cases with coarse aerosol and liquid water cloud models, except low optical depth, while the TMS showed better results in case of ice cloud.

Key words

Radiative transfer algorithms, discrete ordinate method, anisotropic part, large particles.

1. Introduction

This paper continues analysis of the scalar radiative transfer equation (RTE) with highly asymmetric phase function in the framework of discrete ordinates method (DOM) (*Chandrasekhar*, 1950; *Stamnes* and *Swanson*, 1981). In our recent paper (*Korkin et. al*, 2011), a particular attention was paid to the methods based on decomposition of the diffuse light field into a smooth (regular) part and analytically expressed anisotropic part without truncation of the phase function. With anisotropy subtraction, the regular part of the signal, which requires a numerical solution, is essentially smoothed as a function of angles.

In DOM, the view zenith angle (VZA) anisotropy of the signal is expressed via an even number $2N$ of linear differential equations in the system. Each ordinate corresponds to one equation, and there are N ordinates per hemisphere. The azimuthal dependence of radiance is expressed via *Fourier* series with M harmonics, where the system of N linear equations is solved independently for each $m = 0 \dots M$ (Thomas and Stamnes, 1999) providing solution in $i = 1 \dots N$ discrete points $-1 < \mu_i < +1$; $\mu_i \neq 0, \pm 1$.

Our previous work (Korkin et. al, 2011) showed that anisotropy subtraction using a Small-Angle Modification of RTE, implemented in code DOMAS, accelerated azimuthal convergence of solution significantly, by a factor of 3. However, contrary to our expectations, this method did not improve convergence in zenith angle, meaning that a large number of streams would still be required for high accuracy computations with very asymmetric phase functions. It's worth mentioning that accuracy comparison for different number of streams N in (Korkin et. al, 2011) used cubic spline interpolation to yield solution at selected angles. This method was criticized by Karp (1981) as limiting the computational accuracy. A convenient form of computation for an arbitrary angle using integration of the source function was introduced in DOM by Kourganoff (1952). The current work employs the idea of “natural” interpolation by including the required view angles as dummy nodes $-1 \leq \mu_d \leq +1$ into DOM scheme with zero weighting coefficients $w_d = 0$ (Chalhoub and Garcia, 2000). This new approach yields the high accuracy solution with low number of streams. Below, we provide code details and a comparison with other approaches for three cases with high scattering anisotropy, including coarse aerosol fraction and liquid water and ice cloud models.

This paper is structured as follows: Section (2) defines the problem and describes the main characteristics of the methods compared in the paper. The definition of the scenarios for numerical tests is given in Section (3) followed by discussion of the results in Section (4). The paper is concluded with the summary.

2. Definition of the problem

For simplicity, we consider the boundary problem for the scalar RTE and plane-parallel homogeneous atmosphere illuminated at the right angle (Chandrasekhar, 1950)

$$\begin{cases} \mu \frac{\partial I(\tau, \mu)}{\partial \tau} + I(\tau, \mu) = \frac{\omega_0}{2} \int_{-1}^1 p(\mu, \mu') I(\tau, \mu') d\mu' + \frac{\omega_0}{2} p(\mu, 1) \exp(-\tau), \\ I(\tau, \mu^+) = 0; I(\tau_0, \mu^-) = 0. \end{cases} \quad (1)$$

Here, $I(\tau, \mu)$ is the radiance given as a function of optical depth τ ($0 \leq \tau \leq \tau_0$) and a cosine of VZA $\mu = \cos\theta$. The surface is assumed to be black. The media scattering properties are given by

the single scattering albedo ω_0 and phase function $p(\mu, \mu')$. Z-axis is pointed downwards, so that $0^\circ \leq \theta < 90^\circ$ ($\mu^+ > 0$) and $90^\circ < \theta \leq 180^\circ$ ($\mu^- < 0$) correspond to transmitted and reflected radiation, respectively.

The phase function is expanded in Legendre series

$$p(\mu, \mu') = \sum_{k=0}^{K_{max}} (2k+1)x_k P_k(\mu)P_k(\mu'), \quad (2)$$

where $P_k(\mu)$ is the Legendre polynomial of degree k , x_k are expansion moments, and K_{max} is the maximum expansion order necessary for accurate representation of the phase function which will be denoted hereafter as K if the number of term involved is less than K_{max} .

The discrete ordinate method is often used to solve Eq.(1). Using the double-Gauss quadrature (Sykes, 1951), the scattering integral in Eq.(1) is expressed as a sum in the form

$$\int_{-1}^1 p(\mu, \mu') I(\tau, \mu') d\mu' \approx \sum_{j=1}^N w_j p(\mu, \mu_j^-) I(\tau, \mu_j^-) + \sum_{j=1}^N w_j p(\mu, \mu_j^+) I(\tau, \mu_j^+), \quad (3)$$

where w_j are the weighting coefficients, μ_j are the nodes (zeros) of the Legendre polynomial $P_N(\mu)$. Equation (3) yields the system of $2N$ linear differential equations for Eq.(1). While parameters K in Eq.(2) and N in Eq.(3) seem to be independent, it was shown that $N = K/2$ gives numerically stable results (Thomas and Stammes, 1999). Thus $N = K/2$ is assumed in Section 2.

The right-hand side of the RTE Eq.(1) is called the source function (Chandrasekhar, 1950). The free term of the source function contains all K_{max} moments of the phase function

$$\frac{\omega_0}{2} p(\mu, 1) \exp(-\tau) = \frac{\omega_0}{2} \exp(-\tau) \sum_{k=0}^{K_{max}} (2k+1)x_k P_k(\mu)P_k(1), \quad (4)$$

regardless of the number of moments K of the phase function under the scattering integral. The acronym DOM will be used further in this paper for the traditional discrete ordinate method defined by Eqs.(1) - (4) without any modifications. Note, that for the azimuthally independent case the single scattered radiation is included in DOM exactly.

Large particles as in clouds, snow, coarse aerosol fraction etc. cause a strong forward scattering and peaks in the backscattering directions. In these cases, K -parameter in Eq.(2) is large, $\sim 10^3$ as well as the number $2N$ of DOM equations. At large N , the matrix of the system easily becomes ill-conditioned, and its solution is time consuming.

Presently, there are two main approaches to solve the RTE problem with high scattering anisotropy. The first one uses different truncation approximations of phase function. These methods were recently analyzed by Rozanov and Lyapustin (2010). The error caused by truncation of the phase function is significantly reduced by the postprocessing correction in the single scat-

tering (Nakajima and Tanaka, 1988; Muldashev et al., 1999) or the source function integration (Dave and Armstrong, 1974). The second approach singles out the anisotropic part of the light field without changing the phase function (Romanova, 1962; Irvine, 1968; Budak et al. 2010).

In this paper we compare three different methods. The first one singles out the anisotropic part of radiance, $I_A(\tau, \mu)$, using the Small-Angle Modification (Gaudsmit and Saunderson, 1940; Budak and Sarmin, 1990):

$$I(\tau, \mu) = I_A(\tau, \mu) + I_R(\tau, \mu). \quad (5)$$

Importantly, $I_A(\tau, \mu)$ has an analytical expression. With major anisotropy of signal thus removed, the RTE for the smooth regular part, $I_R(\tau, \mu)$, becomes more amenable for the numerical solution than the original Eq. (1). The resulting code DOMAS was described in (Korkin et al., 2011).

In the second method the single scattering approximation is treated as the anisotropic part $I_A(\tau, \mu) = I_1(\tau, \mu)$ (van de Hulst, 1948; Sobolev, 1975)

$$I(\tau, \mu) = I_1(\tau, \mu) + I_{2+}(\tau, \mu) \quad (6)$$

The second and the higher scattering orders, taken together, represent the regular part in this case: $I_R(\tau, \mu) = I_{2+}(\tau, \mu)$. The computational details of this method, called DOM2+, were also given in (Korkin et al., 2011). Eqs.(5) and (6) transform the RTE boundary problem as follows (Lenoble, 1985)

$$\begin{cases} \mu \frac{\partial I_R(\tau, \mu)}{\partial \tau} + I_R(\tau, \mu) = \frac{\omega_0}{2} \int_{-1}^1 p(\mu, \mu') I_R(\tau, \mu') d\mu' + Q\{I_A(\tau, \mu)\}, \\ I_R(\tau, \mu^+) = 0; I_R(\tau_0, \mu^-) = -I_A(\tau_0, \mu^-). \end{cases} \quad (7)$$

Following Eq.(4), the free term of the source function, $Q\{I_A(\tau, \mu)\}$, contains the exact phase function (Eq.(2)) with all K_{max} moments included. The number of expansion moments K of the phase function under the scattering integral should be taken equal to the number of ordinates $2N$ on sphere.

Finally, the third method used in this work is TMS (Nakajima and Tanaka, 1988). TMS uses Delta-M truncation approach (Wiscombe, 1977) and a postprocessing routine to correct the single scattering solution. In the framework of Delta-M method, the RTE boundary problem Eq.(1) is solved using the scaled optical depth and SSA

$$\tau^* = (1 - \omega_0 f)\tau, \quad \omega_0^* = (1 - f)\omega_0 / (1 - \omega_0 f), \quad (8)$$

as well as truncated phase function with $K < K_{max}$ moments, which is also renormalized as:

$$p^*(\mu, \mu', K) = \sum_{k=0}^K (2k+1)x_k^* P_k(\mu) P_k(\mu'), \quad x_k^* = (x_k - f)/(1-f). \quad (9)$$

In Eqs. (8) and (9), f is the first truncated moment of the phase function, $f = x_{K+1}$. If $K = K_{max}$ then $f = 0$. The number of considered moments, K , is twice the number of streams N per hemisphere. Unlike in Eqs.(1) and (7), Delta-M method uses K moments of the phase function both under the scattering integral and in the free term of the source function Eq.(4).

In order to obtain the angular distribution of the radiance, TMS uses the following routine

$$I(\tau, \mu) \approx I_{TMS}(\tau, \mu) = I_{\delta-M}(\tau^*, \omega_0^*, p^*, \mu) - I_1(\tau^*, \omega_0^*, p^*, \mu) + I_1(\tau^*, \omega_0^{TMS}, p, \mu), \quad (10)$$

where $I_{\delta-M}(\tau^*, \omega_0^*, p^*, \mu)$ and $I_1(\tau^*, \omega_0^*, p^*, \mu)$ are the Delta-M and single scattering solutions of Eq.(1), respectively, with optical parameters and phase function p^* given by Eqs.(8) and (9) respectively. $I_1(\tau^*, \omega_0^{TMS}, p, \mu)$ is the solution of Eq.(1) in the single scattering approximation with optical depth τ^* scaled following Eq.(8), rescaled single scattering albedo $\omega_0^{TMS} = \omega_0/(1-\omega_0 f)$, and the exact phase function p given by Eq.(2). *Rozanov and Lyapustin (2010)* found that the TMS method provides the best overall accuracy for the intensity computations among different techniques based on truncation of the phase function.

In this work, we used previously developed codes DOMAS and DOM2+ upgraded with the dummy node interpolation technique described above. For comparison, we also used our own straightforward implementation of DOM (Eqs.(1) and (4)) and of TMS instead of commonly used codes DISORT (ftp://climate1.gsfc.nasa.gov/wiscombe/Multiple_Scatt/) or Rstar (<http://www.ccsr.u-tokyo.ac.jp/~clastr/>). All DOM-based codes feature standard numerical techniques including a singular-value decomposition (*Karp et al., 1980; Stamnes and Swanson, 1981*) and a scaling transformation (*Karp et al., 1980*) for conditioning the matrix of the system. The codes DOMAS, DOM2+, and DOM were tested in our previous paper (*Korkin et al., 2011*). Our implementation of the TMS method was tested against DOM by assuming $K = K_{max}$ (no truncation). The observed agreement was within the computational accuracy.

After definition of scenarios in Section 3, these three approaches, Eqs.(5), (6) and (10), are analyzed in Section 4. The traditional approach of solving RTE Eq.(1) is discussed as well.

3. Definition of Test Cases

The accuracy of the methods was investigated using three types of phase functions with different scattering anisotropy. The first two cases are defined in the code comparison study of *Kokhanovsky (2010)*. A lognormal size distribution at wavelength $\lambda=412$ nm were used for both of these cases. The expansion moments are available at www.iup.physik.uni-bremen.de/~alexk.

The first case represents the coarse aerosol fraction with effective radius $r_o = 0.3\mu\text{m}$, variance $\sigma = 0.92\mu\text{m}$, real refractive index $m = 1.339$, and size integration limits $\Delta r = 0.005\mu\text{m} \dots 30\mu\text{m}$. The case is characterized by the average scattering cosine $x_1 = 0.79$ and $K_{max} = 917$ (918 total, see Eq.(2)).

The second case represents the cloud with the following parameters: $r_o = 5\mu\text{m}$, $\sigma = 0.4\mu\text{m}$, $m = 1.339$, $\Delta r = 0.005\mu\text{m} \dots 100\mu\text{m}$, $x_1 = 0.86$ and $K_{max} = 1671$.

The third case represents the cirrus cloud or snow crystals based on the model of random fractal crystals (Mishchenko et al., 2006, pp.352-353). The expansion moments are available at <http://www.giss.nasa.gov/staff/mmishchenko/brf/>. For this model the power law distribution of project-area-equivalent-sphere radii was assumed (Mishchenko et al., 2006, p.128, Eq.(5.3.14)) with $r_o = 50\mu\text{m}$, $\sigma = 0.2\mu\text{m}$, $m = 1.311$, $\lambda=650\text{nm}$, $x_1 = 0.75$, and $K_{max} = 1999$. The phase functions for the defined three cases are shown in Figure 1.

The results were analyzed for a nearly conservative case $\omega_0 = 1 - 10^{-6}$ and a wide range of optical depth $\tau_0 = 0.1, 1, 10$ for each of the phase functions.

The relative error $\varepsilon(\tau, \mu)$, %, as a function of VZA was the focus of our analysis:

$$\varepsilon(\tau, \mu) = \frac{|I_e(\tau, \mu) - I(\tau, \mu)|}{I_e(\tau, \mu)} 100\%, \quad (11)$$

where $I_e(\tau, \mu)$ is the “exact solution”. The “exact solution” is defined as the solution of the boundary problem, Eq.(1), with all $K_{max}+1$ terms of the phase function taken into account, and with $2N = K_{max}+1$ streams in Eq.(3). Namely, $2N = 918, 1672, 2000$ was assumed for the aerosol, water cloud and ice cloud respectively.

Note that $N = 240$ streams per hemisphere, Delta-M, and single scattering correction were used for the same aerosol case in SCIATRAN code in the benchmark test of codes (Kokhanovsky et al., 2010) that included polarization effects. $N = 180$ streams were assumed for Pstar in order to generate accurate results for aerosol scattering. For the cloud case SCIATRAN used $N = 360$ streams and Pstar used $N = 180$ streams. No significant difference was reported between SCIATRAN and Pstar. In our case, all expansion moments were used for the aerosol and cloud case ($2N = 918$ and 1672), respectively, to generate the baseline solution using standard code DOM. The obtained “exact solutions” for the three cases are plotted in Figure 2 as functions of τ_0 and VZA.

4. Results and Discussion

The results of analysis for the aerosol, liquid water and ice cloud models are presented in Figures 3-5, respectively. They show the logarithm of relative error as a function of τ_0 and VZA

for the transmitted ($VZA = 0^\circ \dots 80^\circ$) and reflected ($VZA = 100^\circ \dots 180^\circ$) radiance for codes DOMAS, TMS, and DOM2+. The results for DOM as compared with the exact solution are given for the reference as well. The results are displayed for two cases $N = 16$ and 32 to show the convergence of solution. The figures show that code DOMAS has a significant advantage over other methods in the aureole area. Even for the most difficult case of ice crystals (Figure 5), the relative error of DOMAS does not exceed 0.1% for $N = 32$. One exception is the case with low optical depth $\tau_0 = 0.1$ where DOM2+ has a more accurate result.

Note, that the obtained results for DOM2+ demonstrate the systematical error component similar to the standard DOM but with significantly smaller values. It shows that using the single scattering field as a source leads to regular part which is not "enough regular". Truncation of the regular part of DOM2+ using the Delta-M technique may improve the performance of DOM2+.

For all considered cases, the error of TMS in the sun direction was relatively high. For the particular case of ice crystals and $N = 32$, the error reached 4%, 40%, and 2000% at $\tau_0 = 0.1$, 1 and 10 respectively. For the aerosol case, it was 0.7%, 4%, and 12% for the same optical depths at $N = 32$. The described error of TMS in the aureole area may slightly affect the accuracy in other directions if the surface reflection is considered.

Outside of the aureole region, DOMAS and TMS provide a generally comparable accuracy for both reflected and transmitted radiance. For example, DOMAS performs slightly better overall for the aerosol and liquid cloud cases, while TMS shows a better accuracy for the case of ice crystals, especially at low optical depth $\tau_0 = 0.1$.

As a summary of this analysis, an average error over all angles,

$$\bar{\varepsilon}(\tau) = \frac{1}{L} \sum_{i=1}^L \varepsilon(\tau, \mu_i), \quad (12)$$

is provided in Tables 1, 2, and 3 for the aerosol case and liquid water and ice cloud models, respectively. The tables show additional results with different number of streams $N = 8$ and 64 than those presented in figures. The average represents $L = 81$ values with 1 degree step for $0^\circ \leq SZA \leq 80^\circ$ for the transmitted radiation and $100^\circ \leq SZA \leq 180^\circ$ for the reflected tradition. The overall best result is highlighted in gray.

In case with coarse fraction of aerosol (Tables 1b, c), DOMAS provided the best result for any considered number of streams and any optical depth, except for the thin layer ($\tau_0 = 0.1$, Table 1a), where DOM2+ was on average the best for any number of streams. Also, DOM2+ is a perfect method for the case of thin water cloud and low (8, 16) number of streams (Table 2a).

In cases with water and ice clouds, moderate ($\tau_0 = 1$, Tables 2b and 3b) and high ($\tau_0 = 10$, Tables 2c and 3c) optical depths, and low number of streams (8, 16), TMS provided the most accurate results for the reflected radiation. In the same cases, DOMAS was the best for the

transmitted radiation. Note that for the case of ice crystals and 8 streams per hemisphere, TMS was the only method that provided the numerically stable solution. Also, the TMS method provided the best result for 8-32 streams in case with thin ice cloud (Table 3a)

In case with water cloud, 32 and 64 streams, DOMAS showed the best average result both for the transmitted and reflected radiation at moderate and high optical depths (Tables 2b, 2c). In case with ice crystals and large number of streams (64), DOMAS was more accurate only at moderate optical depth (Table 3b) with relatively insignificant improvement over TMS for the reflected radiation. For a thick cloud with ice crystals (Table 3c) TMS and DOMAS provided the best results for the reflectance and transmittance, respectively.

Computational time and memory use are two other important dimensions of numerical codes. Given the number of streams, N , all considered methods solve the system of $2N$ linear equations resulting in the same singular value decomposition part of the codes. The main differences appear in treatment of the source function and the bottom boundary condition.

Let us consider the case of liquid water cloud with $\tau_0 = 10$ and $N = 16$ as an example. The relative error for this case is shown by the red line in Figure 4. The accurate DOM solution with $N=K/2$ streams (DOM(exact)) took 48 seconds in the MathWorks Matlab environment running on Intel Pentium T4300, 2.1GGz machine with 4Gb RAM under Microsoft Windows 7. Assuming this time as 1000 in relative units, the time of the other methods is:

$$\text{DOM(exact)} / \text{DOMAS} / \text{TMS} / \text{DOM2+} / \text{DOM} = 1000 / 16 / 1 / 15 / 2. \quad (13)$$

The TMS method shows the best performance with the single scattering correction taking only 2% of the total time. The computer time generally grows along with the complexity of the source function related computations which amounts to 20%, 63% and 84% of the total time for DOM, DOMAS and DOM2+, respectively.

Conclusions

This paper continued analysis of RTE with strongly anisotropic scattering, comparing approaches based on decomposition of the diffuse light field into a regular and anisotropic part. The TMS method, that uses the Delta-M method for truncation of the phase function along with the single scattering correction, was also included in our analysis. It is shown numerically that with anisotropy subtraction, the regular part of the signal, which requires a numerical solution, is essentially smoothed as a function of view zenith angle. The algorithm DOMAS, that singles out the anisotropic radiance in the forward scattering peak using the Small-Angle Modification of RTE, gives accurate results in the aureole area where TMS was shown to have a peak of error. If the reflecting ground surface is considered, this peak of error reduces the accuracy of the result at any view zenith angle beyond the aureole area. Outside of the aureole area, the convergence and

accuracy of DOMAS and TMS is found to be approximately similar: DOMAS was found more accurate in cases with coarse aerosol and liquid water cloud models, except low optical depth, while the TMS showed better results in case of ice clouds. In case with optically thin aerosol layer or water cloud, DOM2+ showed accurate results for a low number of streams.

The memory requirement is found comparable for all of the discussed methods. The best computational efficiency has been demonstrated by the TMS method due to the analytical simplicity of the source function.

Acknowledgements

The first author thanks Dr. Aliaksandr Sinyuk (SSAI and NASA GSFC) for valuable discussions during this work.

References

1. Budak V.P., Sarmin S.E., 1990: Solution of the radiative transfer equation by the method of spherical harmonics in the small-angle modification. *Atm. and Oceanic Optics*, **3**, pp.898-903.
2. Budak V.P., Klyuykov D.A., Korkin SV., 2010: Convergence acceleration of radiative transfer equation solution at strongly anisotropic scattering. In: Kokhanovsky AA, editor. *Light Scattering Reviews 5. Single Light Scattering and Radiative Transfer*. Chichester: Springer; p. 147–204.
3. Chalhoub E.S., Garcia R.D.M., 2000: The equivalence between two techniques of angular interpolation for the discrete-ordinates method. *JQSRT*, **64**, pp. 517-535.
4. Chandrasekhar S., 1950: *Radiative transfer*. Oxford University Press.
5. Dave J.V., Armstrong B.H., 1974: Smoothing of the intensity curve obtained from a solution of the spherical harmonics approximation to the transfer equation. *J. Atmos. Sci.*, **13**, N7, pp.1934 – 1937.
6. Goudsmit S., Saunderson J.L., 1940: Multiple Scattering of Electrons. *Phys.Rev.*, **57**, pp. 24-29.
7. van de Hulst H.C., 1948: Scattering in planetary atmosphere. *Astroph. J.*, **107**, pp.220 – 246.
8. Irvine W.M., 1968: Diffuse reflection and transmission by cloud and dust layers. *JQSRT*, **8**, pp.471–485.
9. Karp A.H., Greenstadt J., Fillmore J.A., 1980: Radiative transfer through an arbitrary thick scattering atmosphere. *JQSRT*, **24**, pp.391–406.
10. Karp A.H., 1981: Computing the angular dependence of the radiation of a planetary atmosphere. *JQSRT*, **25**, pp.403 – 412.
11. Kokhanovsky A.A., Budak V.P., Cornet C., Duan M., Emde C., Katsev I.L., Klyukov

- D.A., Korkin S.V., C-Labonnote L., Mayer B., Min Q., Nakajima T., Ota Y., Prikhach A.S., Rozanov V.V., Yokota T., Zege E.P., 2010: Benchmark results in vector atmospheric radiative transfer. *JQSRT*, **111**, pp.1931-1946.
12. Korkin S.V., Lyapustin A.I., Rozanov V.V., 2011: Analysis of the radiative transfer equation with highly asymmetric phase function. *JQSRT*, **112**, pp.1595 – 1608.
 13. Kourganoff V., 1952: *Basic methods in transfer problems*. Oxford: Clarendon Press.
 14. Lenoble J., Ed., 1985: *Radiative Transfer in Scattering and Absorbing Atmospheres: Standard Computational Procedures*. A. Deepak Publishing.
 15. Mishchenko M.I., Travis L.D., Lacis A.A., 2006: *Multiple scattering of light by particles. Radiative transfer and coherent backscattering*. Cambridge University Press.
 16. Muldashev, T. Z., A. I. Lyapustin, and U. M. Sultangazin, 1999: Spherical Harmonics Method in the Problem of Radiative Transfer in the Atmosphere-Surface System. *JQSRT*, **60**, pp.393-404.
 17. Nakajima T., Tanaka M., 1988: Algorithms for radiative intensity calculations in moderately thick atmospheres using a truncation approximation. *JQSRT*, **40**, N1, pp.51–69.
 18. Romanova L.M., 1962: Solution of the radiative transfer equation in the case of scattering phase function greatly differs from a spherical one. *Opt. Spectrosc.*, **13**, pp.429–435 (in Russian).
 19. Rozanov V.V., Lyapustin A.I., 2010: Similarity of radiative transfer equation: Error analysis of phase function truncation techniques. *JQSRT*, **111**, pp.1964 – 1979.
 20. Sobolev V.V., 1975: *Light Scattering in Planetary Atmospheres*. Pergamon Press.
 21. Stamnes K., Swanson R.A., 1981: A new look at the discrete ordinate method for radiative transfer calculation in anisotropically scattering atmosphere. *J. Atm. Sci.*, **38**, pp.387–399.
 22. Sykes J., 1951: Approximate integration of the equation of transfer. *Mon. Not. Roy. Astron. Soc.* 11, 377 – 386.
 23. Thomas G.E., Stamnes K., 1999: *Radiative transfer in atmosphere and ocean*. Cambridge University Press.
 24. Wiscombe W.J., 1977: The delta-M method: Rapid yet accurate radiative flux calculations for strongly asymmetric phase functions. *J. Atmos. Sci.*, **34**, pp.1408 – 1422.

Table 1a: Mean Relative Error, %, for optical depth $\tau_0 = 0.1$

N	HS	DOM AS	TMS	DOM 2+	DOM
8	μ^-	0.7960	0.4443	0.3766	1.5447
	μ^+	0.1817	0.2352	0.0956	1.5864
6	μ^-	0.2077	0.1472	0.0933	1.1249
	μ^+	0.0504	0.0943	0.0292	0.9198
3	μ^-	0.0270	0.0241	0.0089	0.6735
	μ^+	0.0065	0.0315	0.0048	0.4185
4	μ^-	0.0015	0.0025	0.0003	0.1779
	μ^+	0.0003	0.0110	0.0003	0.1156

Table 1b: Mean Relative Error, %, for optical depth $\tau_0 = 1$

N	HS	DOM AS	TMS	DOM 2+	DOM
8	μ^-	0.3098	0.3254	0.8248	10.823 7
	μ^+	0.0741	1.3031	1.0754	12.832 9
6	μ^-	0.0360	0.1135	0.3726	6.4296
	μ^+	0.0146	0.6164	0.4021	7.5713
3	μ^-	0.0032	0.0383	0.1002	2.8152
	μ^+	0.0012	0.1795	0.1024	3.2824
4	μ^-	0.0005	0.0054	0.0095	0.7921
	μ^+	0.0001	0.0276	0.0094	0.9268

Table 1c: Mean Relative Error, %, for optical depth $\tau_0 = 10$

N	HS	DOM AS	TMS	DOM 2+	DOM
8	μ^-	0.1315	0.0805	6.5087	27.155 4
	μ^+	0.0749	3.8765	10.886 4	35.031 3
6	μ^-	0.0196	0.0279	2.1218	16.513 4
	μ^+	0.0103	0.8915	3.6423	21.481 9
3	μ^-	0.0020	0.0087	0.3288	7.0701
	μ^+	0.0010	0.1745	0.5839	9.2676
4	μ^-	0.0005	0.0012	0.0214	1.9744
	μ^+	0.0001	0.0329	0.0387	2.5949

Accepted manuscript

Table 2a: Mean Relative Error, %, for optical depth $\tau_0 = 0.1$

N	HS	DOM AS	TMS	DOM 2+	DOM
8	μ^-	1.0840	0.2479	0.5959	2.6603
	μ^+	0.2011	0.1758	0.1581	2.5550
6	μ^-	0.4536	0.3181	0.2860	2.1873
	μ^+	0.1120	0.1760	0.0943	2.1805
3	μ^-	0.1504	0.1519	0.0591	3.0376
	μ^+	0.0312	0.1367	0.0529	2.0271
4	μ^-	0.0148	0.1139	0.1140	5.5597
	μ^+	0.0033	0.1664	0.0409	1.9635

Table 2b: Mean Relative Error, %, for optical depth $\tau_0 = 1$

N	HS	DOM AS	TMS	DOM 2+	DOM
8	μ^-	1.5387	0.4384	2.0589	14.708 4
	μ^+	0.2359	1.1369	2.8039	19.476 2
6	μ^-	0.4649	0.3555	2.0003	15.771 2
	μ^+	0.0102	1.1251	2.2606	17.612 2
3	μ^-	0.1324	0.2633	1.9490	13.443 6
	μ^+	0.0219	1.1164	1.8501	15.260 8
4	μ^-	0.0103	0.2727	2.1346	13.330 7
	μ^+	0.0024	0.8652	1.5551	9.6011

Table 2c: Mean Relative Error, %, for optical depth $\tau_0 = 10$

N	HS	DOM AS	TMS	DOM 2+	DOM
8	μ^-	0.7246	0.1508	16.697 7	41.224 1
	μ^+	0.1933	26.485 5	26.915 6	51.994 2
6	μ^-	0.2382	0.1078	14.755 3	38.977 7
	μ^+	0.0296	15.274 2	23.460 1	48.816 7
2	μ^-	0.0514	0.0672	10.115 1	33.946 5

	μ^+	0.0071	5.1885	16.3518	42.8219
4 6	μ^-	0.0048	0.0559	1.8227	18.3400
	μ^+	0.0007	0.6998	3.1250	23.4683

Accepted manuscript

Table 3a: Mean Relative Error, %, for optical depth $\tau_0 = 0.1$

N	HS	DOM AS	TMS	DOM 2+	DOM
8	μ^-	-	0.1179	-	-
	μ^+	-	0.0945	-	-
6	μ^-	1.8685	0.0188	1.2173	2.4418
	μ^+	0.3873	0.0754	0.2593	2.3467
3	μ^-	0.7519	0.0207	0.5628	2.2796
	μ^+	0.1422	0.0724	0.1218	2.3214
4	μ^-	0.1823	0.0109	0.0999	2.3671
	μ^+	0.0350	0.0806	0.0492	2.1538

Table 3b: Mean Relative Error, %, for optical depth $\tau_0 = 1$

N	HS	DOM AS	TMS	DOM 2+	DOM
8	μ^-	-	0.1090	-	-
	μ^+	-	0.8765	-	-
6	μ^-	0.2080	0.0556	2.3336	16.718 2
	μ^+	0.1556	0.7920	2.8423	19.528 0
3	μ^-	0.0981	0.0429	2.0994	16.460 7
	μ^+	0.0763	0.7558	2.7598	19.382 8
4	μ^-	0.0329	0.0360	2.1134	15.719 5
	μ^+	0.0186	0.8193	2.5319	18.042 0

Table 3c: Mean Relative Error, %, for optical depth $\tau_0 = 10$

N	HS	DOM AS	TMS	DOM 2+	DOM
8	μ^-	-	0.0367	-	-
	μ^+	-	46.720 5	-	-
6	μ^-	0.1027	0.0176	17.785 7	42.367 8
	μ^+	0.0766	33.874 8	29.750 2	54.812 4
3	μ^-	0.0538	0.0133	17.203 6	41.799 4
	μ^+	0.0275	27.181 6	29.327 7	54.692 4

4	6	μ^-	0.0254	0.0106	14.937 8	39.136 8
		μ^+	0.0061	16.333 6	27.878 4	51.957 7

Accepted manuscript

Highlights

- (a) DOMAS is accurate in the aureole area even for a low number of streams;
- (b) Beyond the aureole, the accuracy of DOMAS and TMS is similar;
- (c) DOM2+ has a good accuracy for a thin cloud/aerosol layer at a low number of streams;
- (d) All codes have comparable memory requirements, and TMS requires least computer time.

Accepted manuscript

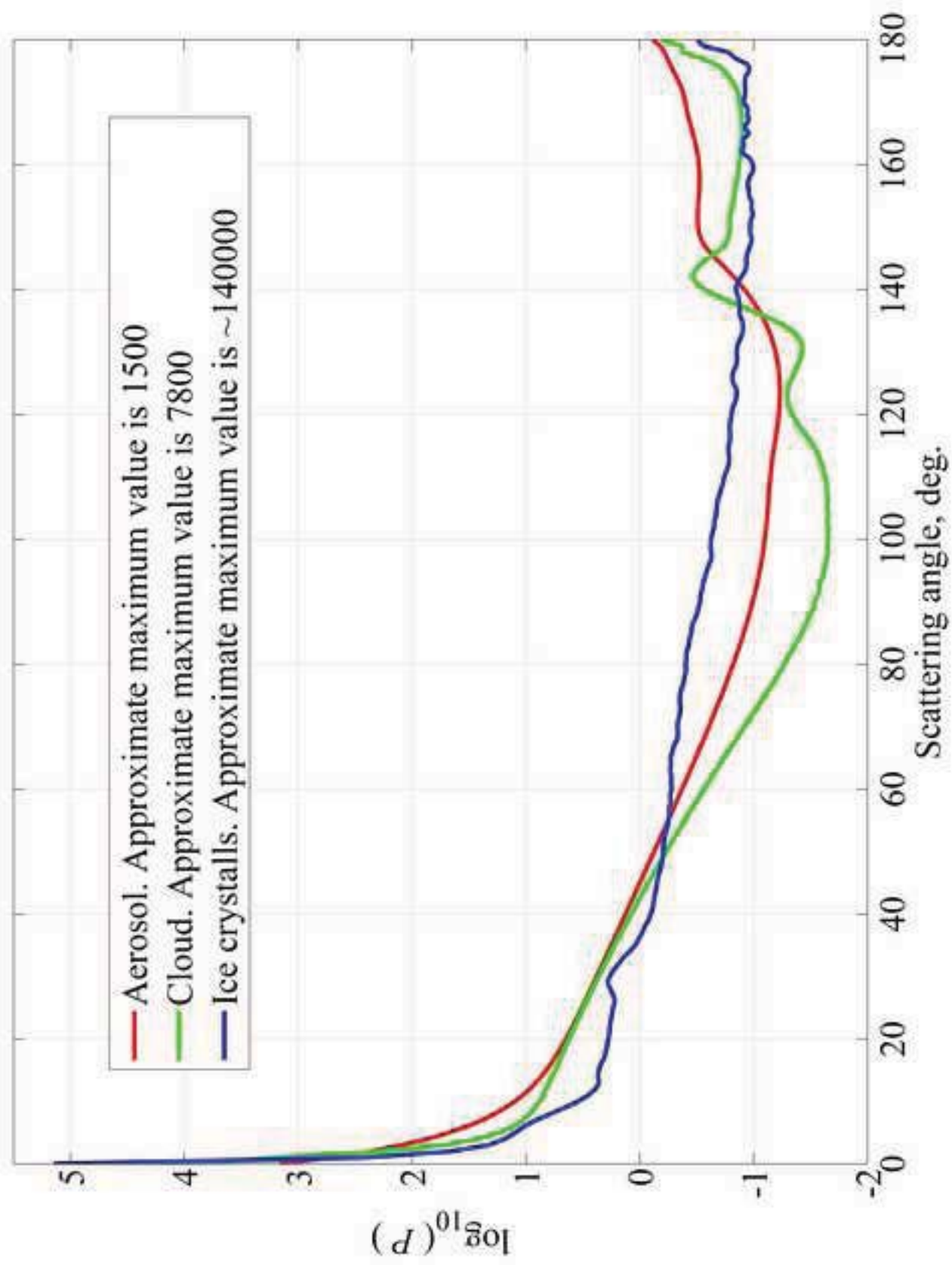
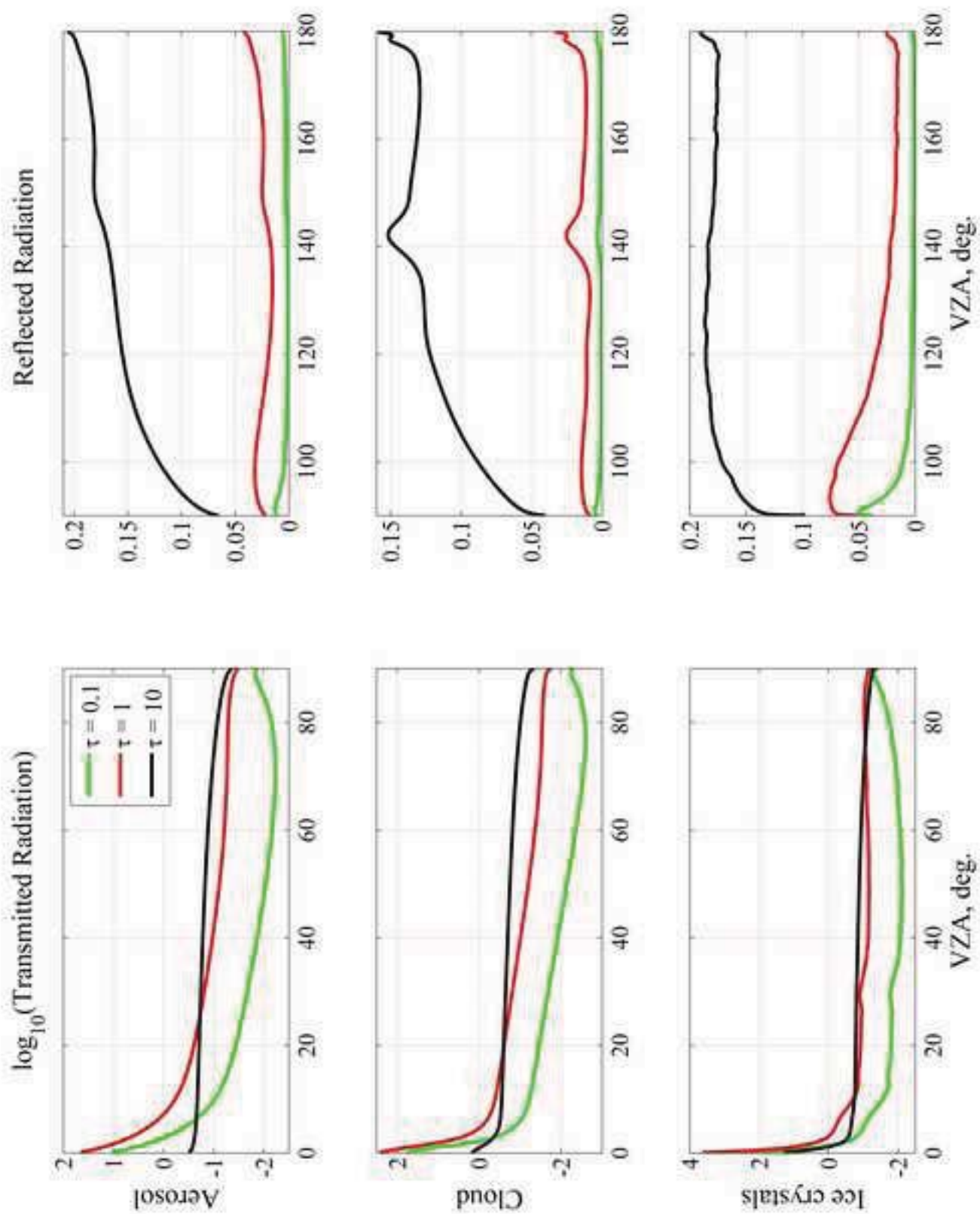
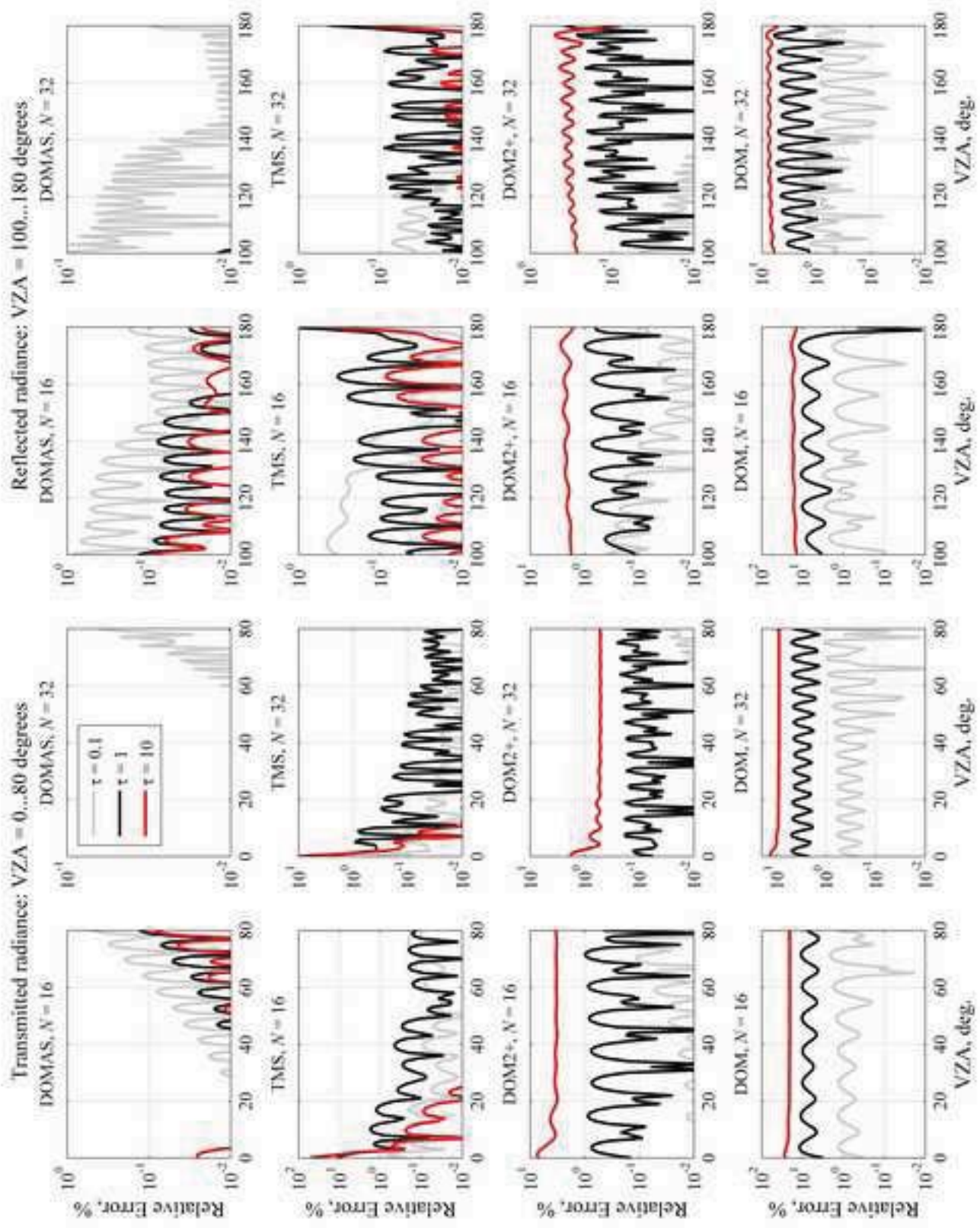
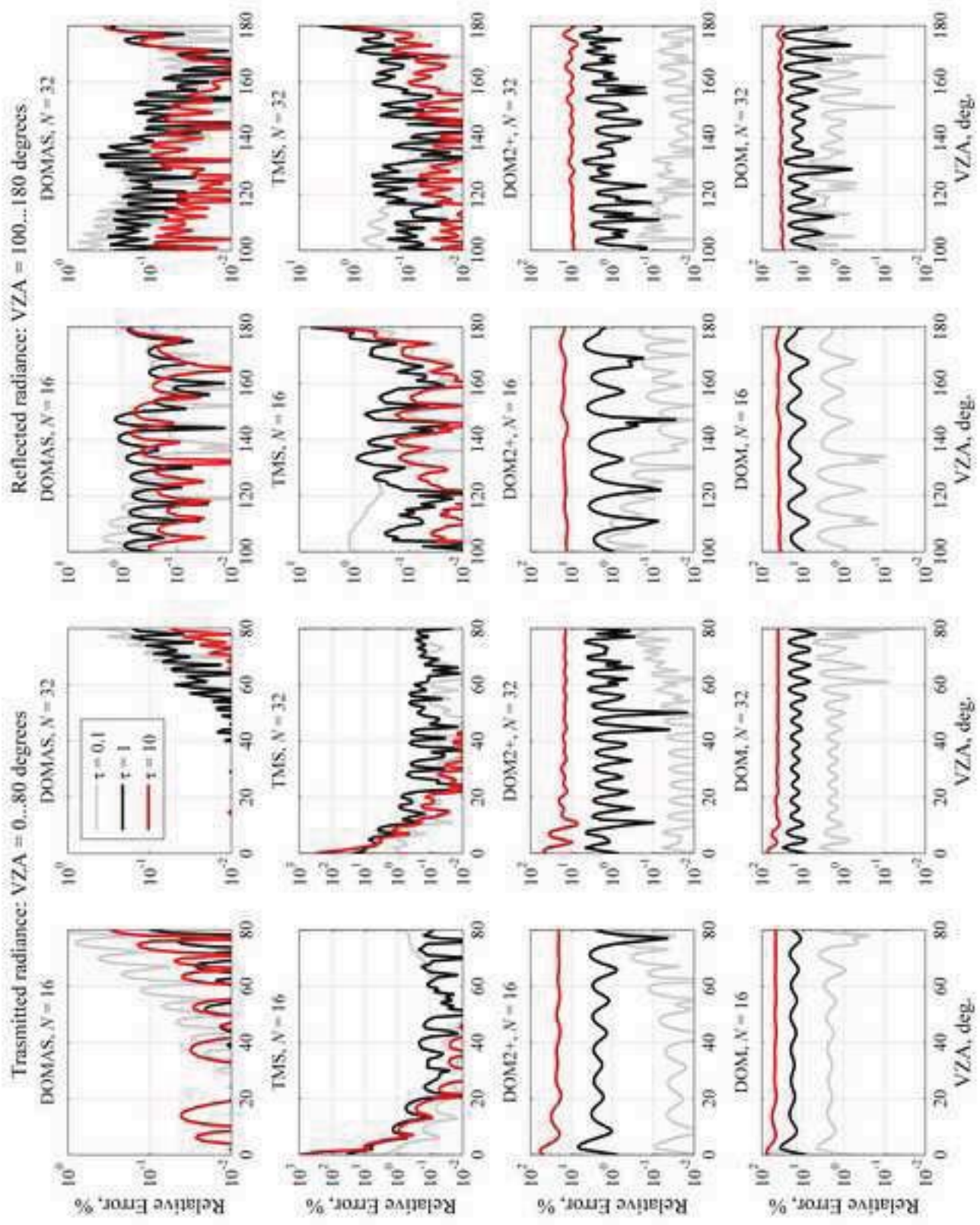


Figure1







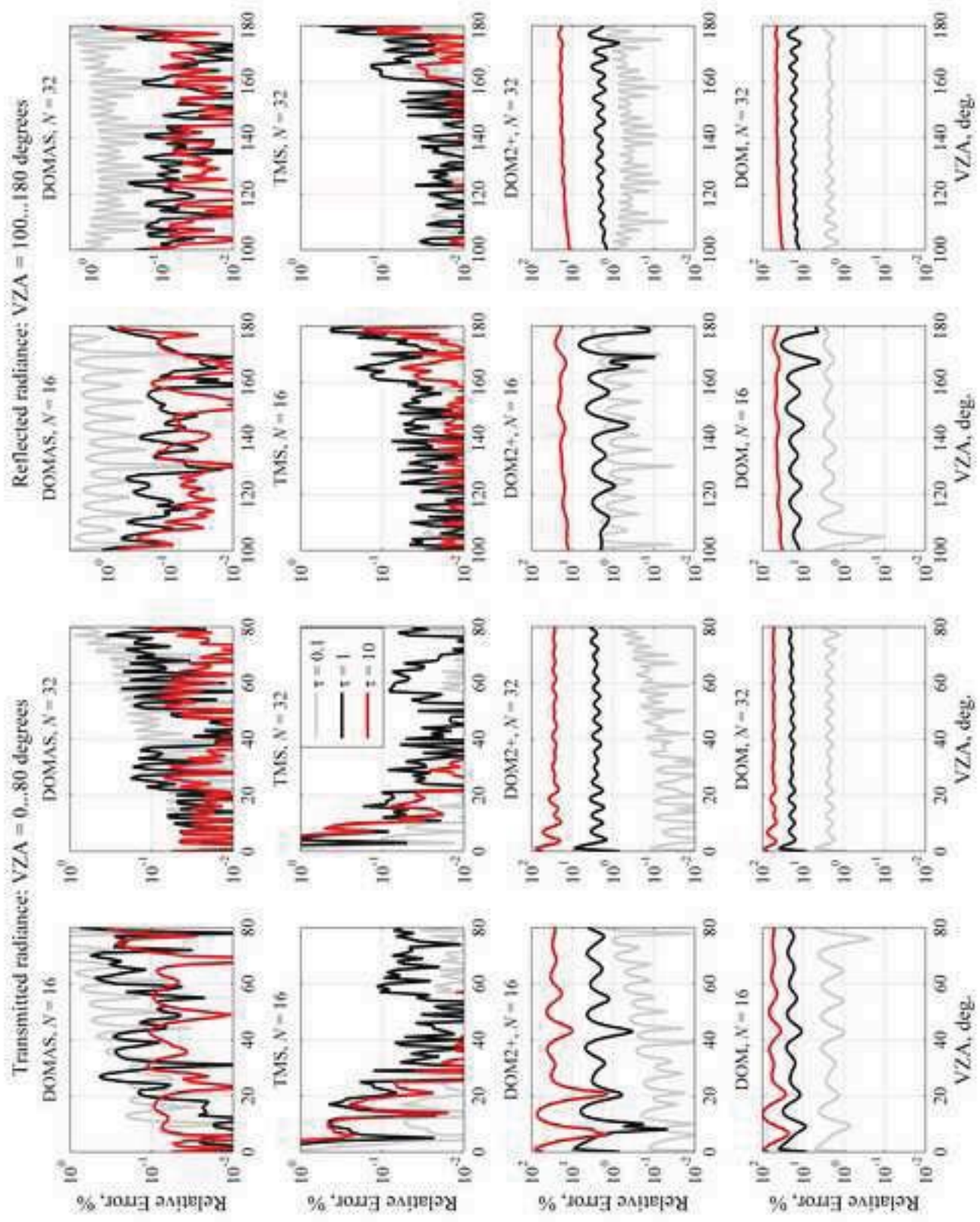


Figure 5